Unscented Kalman filter-based blade-effective wind speed estimation for a vertical-axis wind turbine

Brandetti, Livia; Liu, Yichao; Pamososuryo, Atindriyo K.; Mulders, Sebastiaan P.; Watson, Simon; van Wingerden, Jan Willem

DOI
10.1016/j.ifacol.2023.10.1033

Publication date
2023

Document Version
Final published version

Published in
IFAC-PapersOnLine

Available online at www.sciencedirect.com

ScienceDirect

IFAC Papers Online CONFERENCE PAPER ARCHIVE

IFAC PapersOnLine 56-2 (2023) 8393–8399

Unscented Kalman filter-based blade-effective wind speed estimation for a vertical-axis wind turbine

Livia Brandetti [*,**] **Yichao Liu** [*] **Atindriyo K. Pamososuryo** [*]
Sebastiaan P. Mulders [*] **Simon Watson** [**]
Jan-Willem van Wingerden [*]

[*] *DCSC Department, Faculty of Mechanical, Maritime and Materials Engineering, Delft University of Technology, Delft, The Netherlands (e-mail: {L.Brandetti, Y.Liu-17, A.K.Pamososuryo, S.P.Mulders, J.W.vanWingerden}@tudelft.nl)*

[**] *FPT Department, Faculty of Aerospace Engineering, Delft University of Technology, Delft, The Netherlands (e-mail: {L.Brandetti,S.J.Watson}@tudelft.nl)*

Abstract: On-shore horizontal-axis wind turbines (HAWTs) provide a cost-effective solution for low carbon electricity generation. However, public acceptance is still a problem. A possible alternative to a HAWT is a vertical-axis wind turbine (VAWT), which is more visually appealing and less noisy. Furthermore, the inherent omni-directionality of VAWTs makes them suitable for installation in urban environments where the turbulence levels are high, and the wind direction variations are significant. However, the variation with the azimuth angle of the blade-effective wind speed and the angle of attack makes VAWT performance difficult to predict. This study proposes a wind speed estimator for a VAWT to address this challenge and to exploit knowledge of the blade-effective wind speed for load reduction control strategies. An Unscented Kalman Filter is used to solve the blade-effective wind speed estimation problem and is applied to a realistic 1.5 m two-bladed H-Darrieus VAWT model, for which the aerodynamic characteristics are determined using an actuator cylinder model. The system performance is evaluated using different wind speed variation scenarios. Overall, good agreement between the reference and estimated blade-effective wind speed is found both in terms of trend and absolute values.

Keywords: Blade-effective wind speed, Wind speed estimation, Vertical-axis wind turbine, Kalman filtering, Wind energy

1. INTRODUCTION

The increase in global energy consumption and the need to reduce greenhouse gas emissions have driven the shift from a fossil-fuel-based to a renewable energy-based society. With year-on-year growth of 12 % in installed power capacity, wind plays a key role in the global energy framework (Lee and Zhao, 2022). Offshore wind power capacity in particular has grown rapidly in recent years. The favourable wind resource can be exploited by large offshore wind farms, with an average size of 493 MW (Lee and Zhao, 2022). Onshore sites are still important for future wind power exploitation (Bianchini et al., 2022). Onshore horizontal-axis wind turbines (HAWTs) are a cost-effective solution, however, public acceptance is still a problem (Petrova, 2013).

A promising alternative is a vertical-axis wind turbine (VAWT). A VAWT is intrinsically omni-directional and does not require a yawing system. Also, the location of the generator on the ground leads to easier access and, consequently, lower maintenance costs (Eriksson et al., 2008). Furthermore, VAWTs are visually more appealing and less noisy, making them suitable for installation in urban areas (Graham and Pearson, 2022). The main drawback is their intrinsic three-dimensional aerodynamics due to the variation with the azimuth angle of the blade-effective wind speed (BEWS) and the angle of attack (Simão Ferreira et al., 2009). These periodic and nonlinear system characteristics make the VAWT performance and the wind speed acting on the rotor and blades challenging to predict, especially in urban environments where the turbulence levels are high and the wind direction variations are high (Eriksson et al., 2008).

More accurate wind speed information could facilitate an advanced control algorithm for better load reduction and/or power regulation (Brandetti et al., 2022). In the absence of model uncertainty, the power performance of a 1.5 m two-bladed H-Darrieus VAWT can be maximized by employing a so-called combined wind speed estimator tip-speed ratio (WSE-TSR) tracking controller. This control scheme estimates the rotor-effective wind speed (REWS) based on an extended Immersion and Invariance (I&I) estimator with a Proportional and Integral (PI) correction term (Liu et al., 2022). The REWS estimate is used to estimate the TSR, which in turn is employed as a feedback signal to close the loop by the TSR tracking controller. By acting on the error between the optimal TSR and the

10.1016/j.ifacol.2023.10.1033

TSR estimate, this controller computes a generator torque demand to track the point of maximum power extraction. On the other hand, Individual Pitch Control is a viable solution to minimize the loads on a VAWT's blade (Huijs et al., 2018). With the inclusion of the BEWS estimate, further improvement in load mitigation could be achieved via a feedforward disturbance rejection control paradigm similar to the one developed by Selvam et al. (2009) for a HAWT.

To the authors' knowledge, no BEWS estimation solutions have been proposed for a VAWT. However, based on the one-to-one relation between the blade loads and the BEWS, a load-sensing approach can be developed to estimate this quantity. As demonstrated by Bottasso et al. (2018), knowledge of the out-of-plane bending moments can be exploited to locally estimate the REWS over the rotor-swept area. In this approach, an Extended Kalman Filter (EKF) is applied as a wind speed estimation solution since it allows the use of the linear Kalman Filter equations by linearizing the nonlinear wind turbine dynamics (Soltani et al., 2013).

For a VAWT, using the EKF can lead to complex estimation schemes for the BEWS because the turbine presents highly nonlinear dynamics due to the azimuthal variation of its main parameters. For instance, the loads experience a one-per-revolution periodicity due to the change in BEWS over a rotation. If the assumption of local linearity is violated, the linearisation in the EKF may lead to highly unstable filters (Julier and Uhlmann, 1997). Furthermore, deriving the Jacobian matrices for such complex systems is rather cumbersome. Compared to the EKF, an Unscented Kalman Filter (UKF) can yield equivalent Kalman Filter performance without the linearisation issue (Julier and Uhlmann, 1997).

To this end, the current research aims at BEWS estimation for VAWTs by applying a UKF (Julier and Uhlmann, 1997). Thereby, the main contributions of this paper are:

(1) adapting the WSE-TSR tracking controller presented in (Brandetti et al., 2022) to include the azimuthal variation of the power coefficient by adding the azimuth angle as input of the scheme;
(2) deriving an augmented state-space model for a VAWT that makes use of the blade loads information and employing this as an internal model in the UKF to estimate the BEWS for a VAWT;
(3) assessing the validity of the estimator under different wind speed variation scenarios.

The remainder of this paper is organized as follows: Section 2 provides the assumptions required to apply the WSE-TSR tracking controller and the UKF. Section 3 briefly introduces the VAWT model in which the rotor and blade dynamics are elaborated. The blade-effective estimation problem is addressed and formulated in Section 4, together with the modified WSE-TSR tracking controller. In Section 5, simulation results of the UKF estimator under different wind conditions are presented. Conclusions are drawn in Section 6.

2. ASSUMPTIONS

The first step is formulating the assumptions under which the blade-effective estimation problem is formalized.

Assumption 1. *Throughout this work, the pitch angle β is assumed to be zero as the analysis of the Unscented Kalman Filter is conducted in the below-rated region, where the pitch actuator is inactive.*

Assumption 2. *The azimuth angle θ, the rotor speed ω_r and the normal load on each blade per unit span $F_{n,i}$ are assumed to be measurable. No measurement noise is considered for the azimuth angle.*

Assumption 3. *For simplicity, process and measurement noise $w(k)$ and $v(k)$ are considered uncorrelated zero-mean Gaussian white sequences.*

3. VERTICAL-AXIS WIND TURBINE MODEL

This section derives the vertical-axis wind turbine model used for the formulation of the blade-effective estimation problem. To this end, the two-bladed H-Darrieus Pitch-VAWT turbine is considered, as shown in Fig. 1. To minimize blade deflection, two horizontal struts are used for each blade and are located at approximately 25 % and 75 % of the blade length. The blades have a NACA 0021 profile and a chord of $c_b = 0.075\,\text{m}$, while the struts have a NACA 0018 profile with a chord of $c_s = 0.060\,\text{m}$. The diameter of the VAWT is $D = 1.48\,\text{m}$. The span s and the height H of the VAWT are both equal to 1.5 m. The set-up specifications are summarized in Table 1. More detailed information about the design of the PitchVAWT can be found in previous work (LeBlanc and Simão Ferreira, 2021), in which the turbine was experimentally investigated.

Fig. 1 presents the turbine coordinate system. It is a Cartesian coordinate system with the origin at the turbine

Table 1. PitchVAWT design specifications (LeBlanc and Simão Ferreira, 2021)

Parameter	Value
Number of blades (N_b)	2
Span (s)	1.5 m
Height (H)	1.5 m
Diameter (D)	1.5 m
Blade chord (c_b)	7.5×10^{-2} m
Strut chord (c_s)	6×10^{-2} m
Rated power (P)	6×10^{2} W
Generator efficiency (μ)	1
Gearbox ratio (N)	1
Rotor inertia (J)	1.5 kg m^2

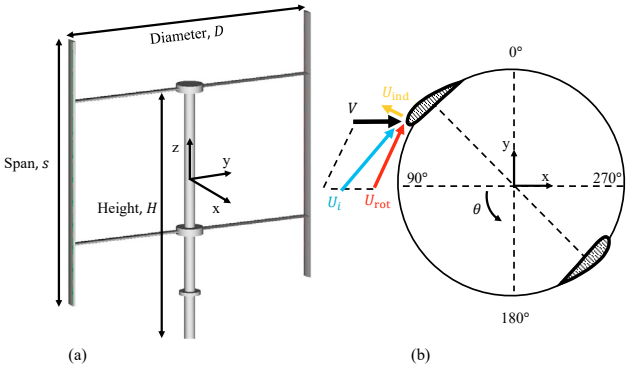

Fig. 1. (a) PitchVAWT geometry and dimensions (b) Coordinate system and definition of the blade-effective wind speed adapted from (De Tavernier, 2021).

center. To further help in the interpretation of the results, the blade orbit is divided into two regions:

- upwind: $0° \leq \theta < 180°$;
- downwind: $180° \leq \theta < 360°$;

with θ being the blade azimuthal position and $\theta = 90°$ and $\theta = 270°$ being, respectively, the most upwind and downwind positions. The azimuthal position is defined with respect to blade 1; therefore, blade 2 lags behind blade 1 by $\theta = 180°$.

By looking at the 2D blade element in Fig. 1, the BEWS for each blade is defined as:

$$\mathbf{U}_i = \mathbf{V} + \mathbf{U}_{\text{rot}} + \mathbf{U}_{\text{ind}}\,, \tag{1}$$

where $i \in N_{\text{b}} = \{1, 2\}$ is the blade index for the VAWT under study, $\mathbf{V}$ is the vector for the REWS, $\mathbf{U}_{\text{rot}}$ is the rotational velocity of the VAWT, which results from the product of the rotational speed ω_{r} and the radius of the turbine R, and $\mathbf{U}_{\text{ind}}$ is the induced velocity, caused by the force field that the turbine generates during the rotation. The interested reader can find a complete derivation of the BEWS in (De Tavernier, 2021).

To solve the blade-effective estimation problem, a first-principle model of the vertical-axis wind turbine is derived in the following subsections by addressing the rotor and blade dynamics.

3.1 Rotor dynamics

The wind turbine rotor dynamics are given by

$$\dot{\theta} = \omega_{\text{r}}\,, \tag{2}$$

$$J\dot{\omega}_{\text{r}} = T_{\text{r}} - T_{\text{g}}N\,, \tag{3}$$

where J is considered at the low-speed shaft (LSS) and is obtained from the relation $J = J_{\text{g}}N^2 + J_{\text{r}}$, in which J_{g} and J_{r} are the inertias of the generator and rotor, respectively, and $N := \omega_{\text{g}}/\omega_{\text{r}}$ represents the gearbox ratio of the transmission with ω_{g} being the generator speed. According to Assumption 1, the aerodynamic rotor torque is given by

$$T_{\text{r}} := \frac{1}{2}\rho A_{\text{rot}}\frac{V^3}{\omega_{\text{r}}}C_{\text{p}}(\lambda, \theta)\,. \tag{4}$$

Here the power coefficient C_{p} is a nonlinear mapping as a function of the tip-speed ratio and azimuth angle

$$\lambda := \frac{\omega_{\text{r}}R}{V}\,. \tag{5}$$

Fig. 2 showcases the C_{p} curves of the considered VAWT, resulting in the nonlinear and periodic behaviour of the aerodynamic torque. The presented mapping is obtained from steady-state wind turbine simulations for a wind profile with a constant velocity of 4 m/s at a range of operating points. As a result of having a two-bladed VAWT, the C_{p} exhibits a twice-per-revolution (2P) periodicity (Lao et al., 2022).

3.2 Blade dynamics

For a vertical-axis wind turbine, the normal load on the blade per unit span is defined as:

$$F_{\text{n},i} = \frac{1}{2}\rho c_{\text{b}}U_i^2 C_{\text{n},i}(\lambda, \theta_i)\,, \tag{6}$$

with U_i being the magnitude of the BEWS for each blade. The normal load coefficient is represented by $C_{\text{n},i}$

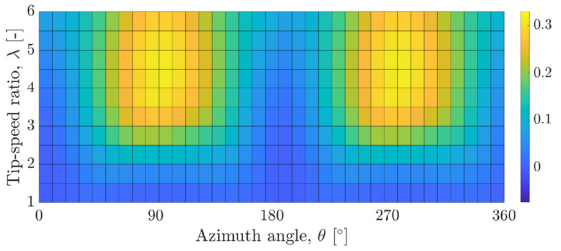

Fig. 2. Power coefficient for the PitchVAWT model for a uniform constant wind speed of 4 m/s.

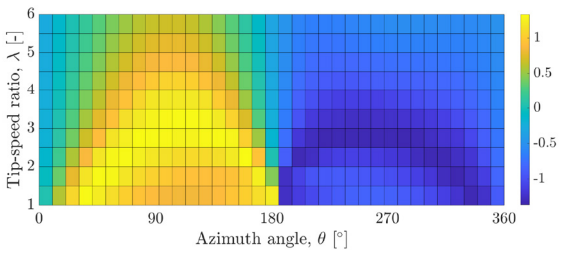

Fig. 3. Normal load coefficient for blade 1 of the Pitch-VAWT model for a uniform constant wind speed of 4 m/s.

and is a nonlinear function of the tip-speed ratio and azimuthal position of blade i. Note that $C_{\text{n},i}$ is also a function of the blade pitch angle β_i, however, in accordance with Assumption 1, β_i is assumed to be constant and equal to 0° throughout this study. Fig. 3 illustrates the $C_{\text{n},1}$ curve for the VAWT model, which is obtained from steady-state wind turbine simulations for a wind profile with a constant velocity of 4 m/s. A maximum normal load can be recognized at around $\theta = 90°$, where blade 1 is upwind. Blade 2 is omitted since it shows similar behaviour. The resulting load dynamics varying through the rotation demonstrate the presence of a once-per-revolution periodicity (1P) on $C_{\text{n},i}$. These periodic dynamics motivate the use of UKF for BEWS estimation since the algorithm is capable of handling nonlinearity up until a third-order Taylor series expansion (Wan and Van Der Merwe, 2000).

In the current work, the aerodynamic data for the look-up tables of C_{p} and $C_{\text{n,i}}$ are obtained using an actuator cylinder model (Madsen, 1982). Based on the defined rotor and blade dynamics, the BEWS estimator problem is formalized in the following.

4. BLADE-EFFECTIVE WIND SPEED ESTIMATOR

This section formulates the blade-effective estimation problem by providing an overview of the general framework and a detailed description of the estimator. As illustrated in Fig. 4, the framework consists of the wind turbine analyzed in Section 3, the modified combined wind speed estimator and tip-speed ratio (WSE-TSR) tracking controller, and the blade-effective wind speed estimator. According to Assumption 2, the red box highlights the real wind turbine system with the generator torque control input, T_{g}, a disturbance input V, and with five outputs: the measured θ, $\tilde{\omega}_{\text{r}}$, $\tilde{F}_{\text{n},1}$ and $\tilde{F}_{\text{n},2}$, and the derived λ. The measured T_{g}, θ and $\tilde{\omega}_{\text{r}}$ are used in the WSE-TSR

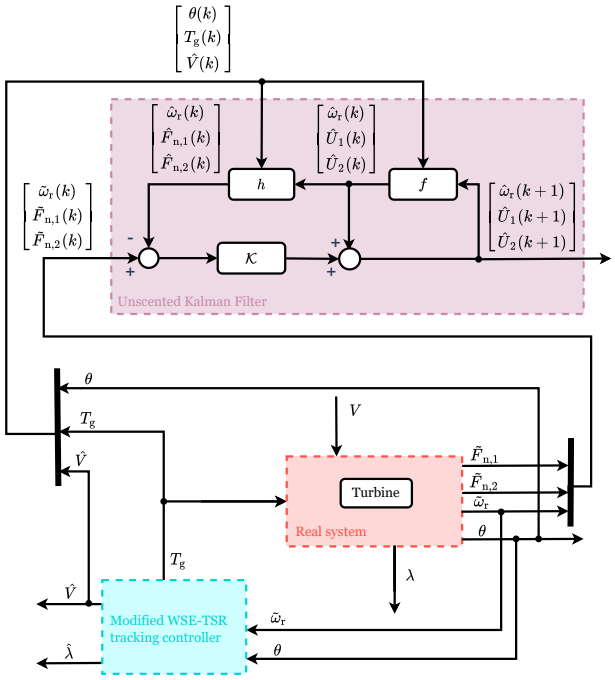

Fig. 4. Block diagram of the blade-effective estimator. The red box contains the wind turbine (i.e. the real system) with azimuth angle θ, tip-speed ratio λ, rotor speed $\tilde{\omega}_\mathrm{r}$ and normal loads on the blades $\tilde{F}_{\mathrm{n},1}$ and $\tilde{F}_{\mathrm{n},2}$ corrupted by measurement noise as outputs, and subjected to a REWS disturbance V and a torque control input T_g computed with the modified WSE-TSR tracker controller (cyan box). The signals $\theta, T_\mathrm{g}, \hat{V}, \tilde{\omega}_\mathrm{r}, \tilde{F}_{\mathrm{n},1}$ and $\tilde{F}_{\mathrm{n},2}$ are used as inputs in the Unscented Kalman Filter (purple block) to make an estimate of the rotor speed $\hat{\omega}_\mathrm{r}$ and of the BEWS of both blades $\hat{U}_1$ and $\hat{U}_2$.

tracking controller to estimate the REWS $\hat{V}$ and the tip-speed ratio $\hat{\lambda}$. In the following subsections, the azimuth extension to the WSE-TSR tracking control scheme, the nonlinear model of the wind turbine and the UKF are presented in detail.

4.1 WSE-TSR tracking controller

This section focuses on modifying the WSE-TSR tracking controller to include the azimuthal variation of the power coefficient. Therefore, only the relevant equations will be provided. The interested reader can find more details on the control scheme in (Brandetti et al., 2022).

The measured $T_\mathrm{g}, \tilde{\omega}_\mathrm{r}$ and θ are used in the extended I&I estimator with a PI correction term (Liu et al., 2022) to estimate the REWS as

$$\begin{cases} J\dot{\hat{\omega}}_\mathrm{r} = \hat{T}_\mathrm{r} - T_\mathrm{g}N \\ \epsilon_{\omega_\mathrm{r}} = \tilde{\omega}_\mathrm{r} - \hat{\omega}_\mathrm{r} \\ \hat{V} = K_{\mathrm{p,w}}\epsilon_{\omega_\mathrm{r}} + K_{\mathrm{i,w}}\int_0^t \epsilon_{\omega_\mathrm{r}}(\tau)\mathrm{d}\tau \end{cases}, \tag{7}$$

with t indicating the present time, τ the variable of integration and $K_{\mathrm{p,w}}$ and $K_{\mathrm{i,w}}$ the proportional and integral estimator gain, respectively. Under Assumption 1, the estimated aerodynamic torque is defined as

$$\hat{T}_\mathrm{r} = \frac{1}{2}\rho A_\mathrm{rot}\frac{\hat{V}^3}{\omega_\mathrm{r}}\hat{C}_\mathrm{p}(\hat{\lambda},\theta)\,, \tag{8}$$

where the estimated power coefficient $\hat{C}_\mathrm{p}$ is a nonlinear function of $\hat{\lambda} := (\tilde{\omega}_\mathrm{r}R)/\hat{V}$ and θ. Thus, it is clear that in this modified form, the WSE-TSR tracking controller allows the 2P periodicity of the C_p in a VAWT to be taken into account.

4.2 Nonlinear state-space model

The wind turbine is represented mathematically by a discrete-time nonlinear state-space model with additive noise,

$$x(k+1) = f(x(k), \mathbf{d}(k), \mathbf{u}(k)) + q(k)\,, \tag{9}$$
$$\mathbf{y}(k) = h(x(k), \mathbf{d}(k), \mathbf{u}(k)) + \mathbf{r}(k)\,, \tag{10}$$

where k is the time index, $x \in \mathbb{R}$ is the system state, $\mathbf{d} \in \mathbb{R}^2$ is the disturbance, $\mathbf{y} \in \mathbb{R}^3$ are the measured outputs of the system, $\mathbf{u} \in \mathbb{R}^3$ are the controllable inputs while $q \in \mathbb{R}$ and $\mathbf{r} \in \mathbb{R}^3$ represent the process noise that drives the system dynamics and the measurement noise, respectively (Wan and Van Der Merwe, 2000). The system dynamic model f and h are known according to the above-mentioned dynamics.

For the case under study, the state is defined as $x = \omega_\mathrm{r}$, the disturbance is $\mathbf{d} = [U_1, U_2]^\mathrm{T}$, the input consists out of $\mathbf{u} = [\theta, T_\mathrm{g}, \hat{V}]^\mathrm{T}$ and the output is $\mathbf{y} = [\tilde{\omega}_\mathrm{r}, \tilde{F}_{\mathrm{n},1}, \tilde{F}_{\mathrm{n},2}]^\mathrm{T}$ (Assumption 2).

By applying a forward Euler technique to (3), the discretised drivetrain dynamics are obtained as follows

$$\omega_\mathrm{r}(k+1) = \omega_\mathrm{r}(k) + \left(\frac{1}{J}T_\mathrm{r}(k) - \frac{1}{J}NT_\mathrm{g}(k)\right)\Delta t + q_\mathrm{p}(k)\,, \tag{11}$$

where Δt is the sampling time and q_p is the process noise for the rotational speed.

It is assumed that the BEWS varies according to the following random-walk model

$$U_i(k+1) = U_i(k) + q_{\mathrm{u},i}(k)\,, \tag{12}$$

in which $q_{\mathrm{u,i}}$ is the process noise for the BEWS of each blade.

Using (3) to (12) and applying Assumption 2, the dynamics of the VAWT are represented by

$$\mathbf{x}^a(k+1) = f(\mathbf{x}^a(k), \mathbf{u}(k)) + \mathbf{q}(k), \tag{13}$$
$$\mathbf{y}(k) = h(\mathbf{x}^a(k), \mathbf{u}(k)) + \mathbf{r}(k), \tag{14}$$

in which $\mathbf{x}^a$ is the augmented state including the disturbance $\mathbf{d}$, and is defined as

$$\begin{bmatrix} \omega_\mathrm{r}(k+1) \\ U_1(k+1) \\ U_2(k+1) \end{bmatrix} = \begin{bmatrix} \omega_\mathrm{r}(k) + \left(\frac{1}{J}T_\mathrm{r}(k) - \frac{1}{J}NT_\mathrm{g}(k)\right)\Delta t \\ U_1(k) \\ U_2(k) \end{bmatrix} + \begin{bmatrix} q_\mathrm{p}(k) \\ q_{\mathrm{u},1}(k) \\ q_{\mathrm{u},2}(k) \end{bmatrix}. \tag{15}$$

The output equation is written as

$$\begin{bmatrix} \tilde{\omega}_\mathrm{r}(k) \\ \tilde{F}_{\mathrm{n},1}(k) \\ \tilde{F}_{\mathrm{n},2}(k) \end{bmatrix} = \begin{bmatrix} \omega_\mathrm{r}(k) \\ \frac{1}{2}\rho c_\mathrm{b} U_1^2(k) C_{\mathrm{n},1}(\lambda, \theta_1(k)) \\ \frac{1}{2}\rho c_\mathrm{b} U_2^2(k) C_{\mathrm{n},2}(\lambda, \theta_2(k)) \end{bmatrix} + \begin{bmatrix} r_\omega(k) \\ r_1(k) \\ r_2(k) \end{bmatrix}, \tag{16}$$

where r_ω, r_1, r_2 are the measurement noise for ω_r and for the normal load of each blade, respectively.

By applying Assumption 3, the covariance of the noise signals can be written as diagonal matrices

$$Q(k) = \mathrm{cov}(\mathbf{q}(k)) = \begin{bmatrix} \sigma^2(q_\mathrm{p}(k)) & 0 & 0 \\ 0 & \sigma^2(q_{\mathrm{u},1}(k)) & 0 \\ 0 & 0 & \sigma^2(q_{\mathrm{u},2}(k)) \end{bmatrix}, \tag{17}$$

$$R(k) = \mathrm{cov}(\mathbf{r}(k)) = \begin{bmatrix} \sigma^2(r_\omega(k)) & 0 & 0 \\ 0 & \sigma^2(r_1(k)) & 0 \\ 0 & 0 & \sigma^2(r_2(k)) \end{bmatrix}, \tag{18}$$

in which $\sigma(\cdot)$ is the standard deviation of the signal. Note that the mean of the process and measurement noise are indicated as $\bar{\mathbf{q}}(k)$ and $\bar{\mathbf{r}}(k)$, respectively.

4.3 Unscented Kalman filter

The following describes the UKF applied to solve the BEWS estimation problem. The Kalman Filter (KF) is used to estimate the state vector of a system using noisy measurements. The UKF is considered an extension of the KF for nonlinear systems and an improvement on the EKF since no linearization is needed (Wan and Van Der Merwe, 2000). The UKF is based on the Unscented Transformation (UT), which uses a set of chosen weighted points, the so-called sigma points, to parameterise the mean and covariance of the probability distribution (Julier and Uhlmann, 1997). With this approach, the UKF can achieve a third-order (Taylor series expansion) accuracy in estimating the posterior mean and covariance, while the EKF only has first-order accuracy (Wan and Van Der Merwe, 2000).

To implement the UKF, the discrete augmented nonlinear system defined in (13) and (14) is used. The first step in the UKF is the initialization of the mean state vector $\bar{\mathbf{x}}^a(0)$ and covariance $\mathbf{P}(0)$ of the augmented state $\mathbf{x}^a$ with dimension $L = 3$.

Then, the state is approximated by $2L + 1$ sigma points $\mathcal{X}_j$ with corresponding weights W_j, defined as

$$\begin{cases} \mathcal{X}_0 & = \mathbf{x}^a \\ \mathcal{X}_j & = \mathbf{x}^a + \left(\sqrt{(L+\gamma)\mathbf{P}}\right)_j \\ & \text{for} \quad j = 1, 2, \ldots, L \\ \mathcal{X}_j & = \mathbf{x}^a - \left(\sqrt{(L+\gamma)\mathbf{P}}\right)_{j-L} \\ & \text{for} \quad j = L+1, L+2, \ldots, 2L \end{cases}, \tag{19}$$

$$\begin{cases} W_0^m & = \gamma/(L+\gamma) \\ W_0^c & = \gamma/(L+\gamma) + \left(1 + \phi - \alpha^2\right) \\ W_j^m & = W_j^c = 1/2(L+\gamma), \quad j = 1, 2, \ldots, 2L, \end{cases}, \tag{20}$$

where $\gamma = \alpha^2(L + \kappa) - L$ is a scaling parameter, $\alpha = 0.001$ determines the spread of the sigma points around $\bar{\mathbf{x}}^a$, $\kappa = 0$ is a secondary scaling parameter, and $\phi = 2$ includes the prior knowledge of the distribution of $\mathbf{x}^a$.

Follows the time update, in which the sample point, the predicted state mean and covariance, and the outputs are predicted by

$$\mathcal{X}_j(k+1|k) = f(\mathbf{x}^a(k+1|k), \mathbf{u}(k)) + \bar{\mathbf{q}}(k)\,, \tag{21}$$

$$\hat{\mathbf{x}}^a(k+1|k) = \sum_{j=0}^{2L} W_j^m \mathcal{X}_j(k+1|k)\,, \tag{22}$$

$$\begin{aligned} \mathbf{P}(k+1|k) = \sum_{j=0}^{2L} W_j^c (\mathcal{X}_j(k+1|k) - \hat{\mathbf{x}}^a(k+1|k)) \\ \times (\mathcal{X}_j(k+1|k) - \hat{\mathbf{x}}^a(k+1|k))^\mathrm{T}\,, \end{aligned} \tag{23}$$

$$\mathcal{Y}_j(k+1|k) = h(\mathbf{x}^a(k+1|k), \mathbf{u}(k)) + \bar{\mathbf{r}}(k)\,, \tag{24}$$

$$\hat{\mathbf{y}}(k+1|k) = \sum_{j=0}^{2L} W_j^m \mathcal{Y}_j(k+1|k)\,, \tag{25}$$

The last step is the measurement update, in which the state $\hat{\mathbf{x}}^a$ and covariance $\mathbf{P}$ are estimated as

$$\hat{\mathbf{x}}^a(k+1) = \hat{\mathbf{x}}^a(k+1|k) + \mathcal{K}\left(\mathbf{y}(k) - \hat{\mathbf{y}}(k+1|k)\right)\,, \tag{26}$$

$$\mathbf{P}(k+1) = \mathbf{P}(k+1|k) - \mathcal{K}\mathbf{P}_{\mathbf{y},\mathbf{y}}\mathcal{K}^\mathrm{T}\,, \tag{27}$$

where $\mathcal{K}$ is the Kalman gain defined as

$$\mathcal{K} = \mathbf{P}_{\mathbf{x},\mathbf{y}}\mathbf{P}_{\mathbf{y},\mathbf{y}}^{-1}\,, \tag{28}$$

with

$$\begin{aligned} \mathbf{P}_{\mathbf{x},\mathbf{y}} = \sum_{j=0}^{2L} W_j^c (\mathcal{X}_j(k+1|k) - \hat{\mathbf{x}}^a(k+1|k)) \\ \times ((\mathcal{Y}_j(k+1|k) - \hat{\mathbf{y}}(k+1|k))^\mathrm{T}\,, \end{aligned} \tag{29}$$

$$\begin{aligned} \mathbf{P}_{\mathbf{y},\mathbf{y}} = \sum_{j=0}^{2L} W_j^c (\mathcal{Y}_j(k+1|k) - \hat{\mathbf{y}}(k+1|k)) \\ \times ((\mathcal{Y}_j(k+1|k) - \hat{\mathbf{y}}(k+1|k))^\mathrm{T}\,. \end{aligned} \tag{30}$$

It can be seen, no explicit calculation of the Jacobians is needed to implement the UKF, which motivates its use for the considered BEWS estimation problem (Wan and Van Der Merwe, 2000). Following the derived steps, the next section will show the results of the UKF applied to the studied VAWT.

5. RESULTS AND DISCUSSIONS

This section presents the simulation results obtained by applying the UKF under different environmental conditions. The framework presented in Section 4 is implemented in Simulink. To evaluate the performance of the estimator, three different case studies are simulated: an ideal constant wind profile, a step-wise increasing wind speed and a realistic turbulent wind field. The process and measurement noise covariances are treated as tuning parameters and summarized in Table 2, together with the other tuning variables used in the UKF. The I&I REWS estimator gains are calibrated as $K_{\mathrm{p,w}} = 2$ and $K_{\mathrm{i,w}} = 5$, resulting in satisfactory estimator performance. The TSR tracking gains $K_{\mathrm{p,c}} = -10$ and $K_{\mathrm{i,c}} = -0.5$ are tuned to achieve a balance between the performance and robustness of the PI controller. Only the results for blade 1 are presented as blade 2 shows similar behaviour.

Table 2. Unscented Kalman Filter settings

Parameter	Value
Process covariance of ω_r $(\sigma^2(q_\mathrm{p}(k)))$	$1 \times 10^{-3}\,\mathrm{rad^2/s^2}$
Process covariance of U_1 $(\sigma^2(q_{\mathrm{u},1}(k)))$	$1 \times 10^{-6}\,\mathrm{m^2/s^2}$
Process covariance of U_2 $(\sigma^2(q_{\mathrm{u},2}(k)))$	$1 \times 10^{-6}\,\mathrm{m^2/s^2}$
Measurement covariance of ω_r $(\sigma^2(r_\omega(k)))$	$1 \times 10^{-7}\,\mathrm{rad^2/s^2}$
Measurement covariance of $F_{\mathrm{n},1}$ $(\sigma^2(r_1(k)))$	$1 \times 10^{-5}\,\mathrm{m^2}$
Measurement covariance of $F_{\mathrm{n},2}$ $(\sigma^2(r_2(k)))$	$1 \times 10^{-5}\,\mathrm{m^2}$
Tuning parameter (α)	1×10^{-3}
Tuning parameter (κ)	0
Tuning parameter (ϕ)	2
Sampling time (Δt)	$1 \times 10^{-3}\,\mathrm{s}$

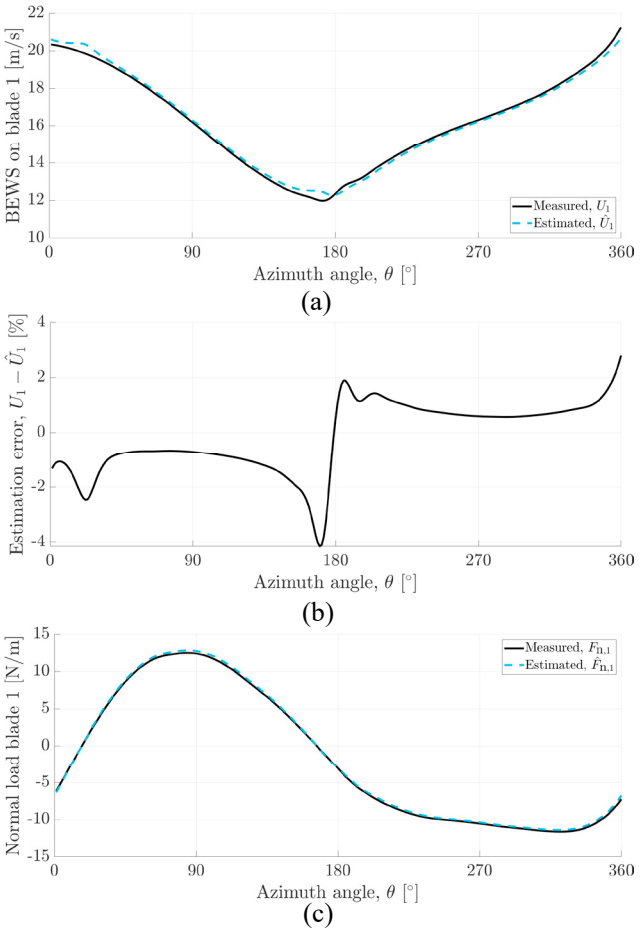

Fig. 5. Estimation results for blade 1 for an ideal constant wind speed of 4 m/s: (a) blade-effective wind speed, (b) relative estimation error, (c) normal load.

5.1 Constant wind case

Since loads on the VAWT vary considerably over a single rotation, it is necessary to present the data in the azimuthal domain to assess the estimator's performance. Fig. 5 illustrates the BEWS, the relative estimation error (i.e. $U_1 - \hat{U}_1$) and the normal load on blade 1. Overall, the UKF correctly predicts the BEWS on blade 1 in terms of trend and absolute values. However, significant differences can be noticed at $\theta = 0°$ and $\theta = 180°$, which represent crucial locations for the VAWT performance. For the former angle, the BEWS has a higher value because the REWS and the U_{rot} are in the same direction. For the latter, the BEWS is minimum because the REWS and the U_{rot} are in opposite directions. As described in Section 3, the normal load $F_{\text{n},1}$ also varies over the rotation, assuming positive values upwind and negative values downwind, with its maximum value at $\theta = 90°$. At this location, the UKF slightly overestimates the normal load on the blade due to the overestimation of the BEWS(see (6)).

5.2 Step-wise wind case

In this case, a wind profile with a step-wise increasing wind speed from 4 m/s to 5 m/s is considered. The step occurs at 200 s. Results for the BEWS and the relative estimation error (i.e. $U_1 - \hat{U}_1$) are illustrated in Fig. 6. At

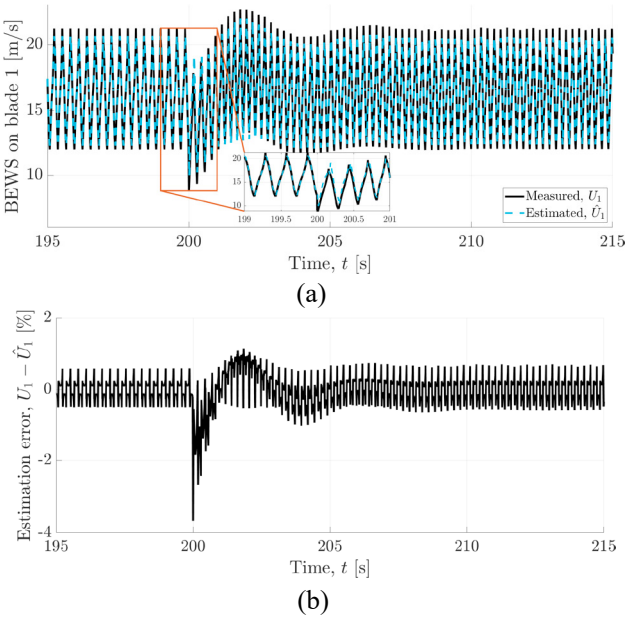

Fig. 6. Estimation results for blade 1 for a step-wise increasing wind speed from 4 m/s to 5 m/s: (a) blade-effective wind speed, (b) relative estimation error.

the transition of a different wind speed step, the BEWS experiences a high overshoot. The UKF is able to follow this change in speed and to reduce the estimation error close to zero in less than 5 s.

5.3 Turbulent wind case

In this case, the wind turbine operates under a realistic turbulent wind field with a mean wind speed of 4 m/s and a turbulence intensity of 20 % for 600 s. Due to the large oscillations induced by the intrinsic periodicity of the turbine, only two small portions of the simulation are presented here. The analysed time frames are emphasised in Fig. 7, where zoom-ins on the estimated REWS are provided together with the corresponding estimations for the BEWS. As can be seen, the trend of the BEWS is correctly estimated with a slight inaccuracy for the critical points previously discussed.

6. CONCLUSION

This study proposes an Unscented Kalman filter-based blade-effective wind speed estimation for a vertical-axis wind turbine. The WSE-TSR tracking controller provides the torque control signal to the turbine and is modified to consider the azimuthal variation of the power coefficient in the VAWT. A first-order nonlinear model was designed to estimate the performance of a realistic 1.5 m two-bladed H-Darrieus VAWT. It is shown that the estimator correctly predicts the blade-effective wind speed of a VAWT under different wind speed variation scenarios, proving that the UKF is able to handle the intrinsic nonlinearity of the VAWT. Due to the one-to-one relationship between the blade-effective wind speed and the blade loads, future work will take advantage of the knowledge of the estimated blade-effective wind speed to develop load reduction strategies for VAWTs by means of Individual Pitch Control.

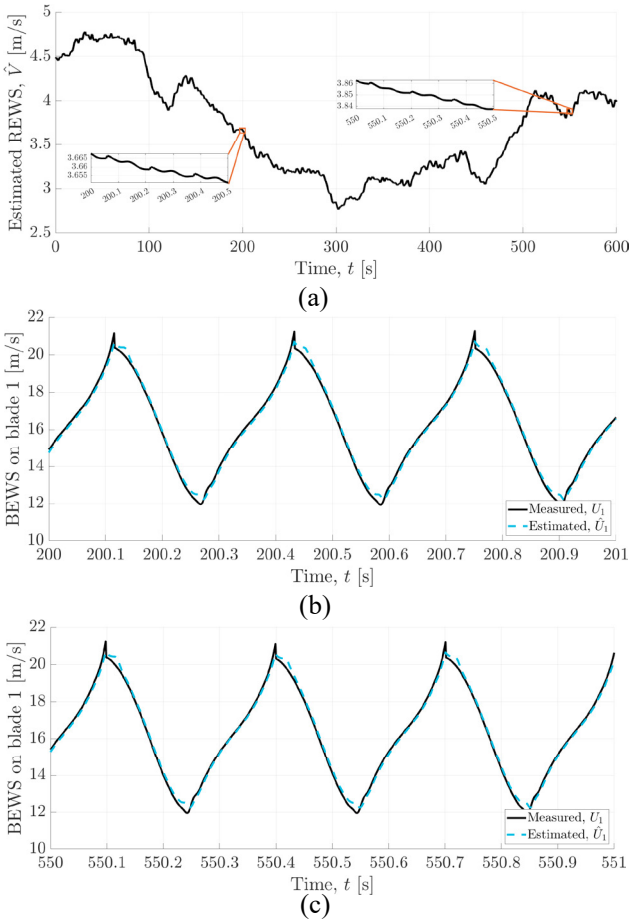

Fig. 7. Estimation results for a realistic turbulent wind profile with a mean wind speed of 4 m/s and a turbulence intensity of 20 %: (a) time traces of the estimated rotor-effective wind speed, (b) and (c) blade-effective wind speed for blade 1 for two different time frames.

REFERENCES

Bianchini, A., Bangga, G., Baring-Gould, I., Croce, A., Cruz, J.I., Damiani, R., Erfort, G., Simão Ferreira, C., Infield, D., Nayeri, C.N., Pechlivanoglou, G., Runacres, M., Schepers, G., Summerville, B., Wood, D., and Orrell, A. (2022). Current status and grand challenges for small wind turbine technology. *Wind Energy Science*, 7(5), 2003–2037. doi:10.5194/wes-7-2003-2022.

Bottasso, C., Cacciola, S., and Schreiber, J. (2018). Local wind speed estimation, with application to wake impingement detection. *Renewable Energy*, 116, 155–168. doi:10.1016/j.renene.2017.09.044.

Brandetti, L., Liu, Y., Mulders, S.P., Ferreira, C., Watson, S., and van Wingerden, J.W. (2022). On the ill-conditioning of the combined wind speed estimator and tip-speed ratio tracking control scheme. Journal of Physics: Conference Series. doi:10.1088/1742-6596/2265/3/032085.

De Tavernier, D.M.A. (2021). *Aerodynamic advances in vertical-axis wind turbines*. Ph.D. thesis.

Eriksson, S., Bernhoff, H., and Leijon, M. (2008). Evaluation of different turbine concepts for wind power. *Renewable and Sustainable Energy Reviews*, 12, 1419–1434. doi:10.1016/j.rser.2006.05.017.

Graham, W.R. and Pearson, C.E. (2022). Noise from a Model-Scale Vertical-Axis Wind Turbine. *AIAA Journal*, 60(1), 224–235. doi:10.2514/1.J060531.

Huijs, F., Vlasveld, E., Gormand, M., Savenije, F., Caboni, M., Leblanc, B., Simão Ferreira, C., Lindenburg, K., Gueydon, S., Otto, W., and Paillard, B. (2018). Integrated design of a semi-submersible floating vertical axis wind turbine (VAWT) with active blade pitch control. Journal of Physics: Conference Series. doi:10.1088/1742-6596/1104/1/012022.

Julier, S.J. and Uhlmann, J.K. (1997). New extension of the Kalman filter to nonlinear systems. Signal Processing, Sensor Fusion, and Target Recognition VI. doi:10.1117/12.280797.

Lao, Y., Rotea, M.A., Koeln, J.P., Sakib, M.S., and Griffith, D.T. (2022). Economic Nonlinear Model Predictive Control of Offshore Vertical-Axis Wind Turbines. 2022 American Control Conference (ACC), 3518–3525. doi:10.23919/ACC53348.2022.9867846.

LeBlanc, B. and Simão Ferreira, C. (2021). Estimation of blade loads for a variable pitch vertical axis wind turbine from particle image velocimetry. *Wind Energy*, 1–20. doi:10.1002/we.2674.

Lee, J. and Zhao, F. (2022). Global Wind Report 2022. Technical report.

Liu, Y., Pamososuryo, A.K., Ferrari, R.M., and van Wingerden, J.W. (2022). The Immersion and Invariance Wind Speed Estimator Revisited and New Results. *IEEE Control Systems Letters*, 6, 361–366. doi:10.1109/LCSYS.2021.3076040.

Madsen, H.A. (1982). *The Actuator Cylinder - A Flow Model for Vertical Axis Wind Turbines*. Ph.D. thesis. doi:10.13140/RG.2.1.2512.3040.

Petrova, M.A. (2013). NIMBYism revisited: Public acceptance of wind energy in the United States. *WIREs Clim Change*, 4, 575–601. doi:10.1002/wcc.250.

Selvam, K., Kanev, S., van Wingerden, J.W., and van Engelen, T. (2009). Feedback – feedforward individual pitch control for wind turbine load reduction. *International Journal Of Robust And Nonlinear Control*, 72–91. doi:10.1002/rnc.1324.

Simão Ferreira, C.J., van Kuik, G., van Bussel, G., and Scarano, F. (2009). Visualization by PIV of dynamic stall on a vertical axis wind turbine. *Experiments in Fluids*, 97–108. doi:10.1007/s00348-008-0543-z.

Soltani, M.N., Knudsen, T., Svenstrup, M., Wisniewski, R., Brath, P., Ortega, R., and Johnson, K. (2013). Estimation of rotor effective wind speed: A comparison. *IEEE Transactions on Control Systems Technology*, 21, 1155–1167. doi:10.1109/TCST.2013.2260751.

Wan, E.A. and Van Der Merwe, R. (2000). The unscented Kalman filter for nonlinear estimation. IEEE 2000 Adaptive Systems for Signal Processing, Communications, and Control Symposium, 153–158. doi:10.1109/ASSPCC.2000.882463.